SAN99-0056C

Submitted to the Renewable and Advanced Energy Conference for the 21st Century Conference
April 1999, Maui, HA.

Heat Pipe Solar Receiver Development Activities at Sandia National Laboratories

D. R. Adkins, C. E. Andraka, J. B. Moreno, K. S. Rawlinson, S. K. Showalter and T. A. Moss
Sandia National Laboratories, Albuquerque, NM 87185

ABSTRACT

Over the past decade, Sandia National Laboratories has been involved in the development of receivers to transfer energy from the focus of a parabolic dish concentrator to the heater tubes of a Stirling engine. Through the isothermal evaporation and condensation of sodium, a heat-pipe receiver can efficiently transfer energy to an engine's working fluid and compensate for irregularities in the flux distribution that is delivered by the concentrator. The operation of the heat pipe is completely passive because the liquid sodium is distributed over the solar-heated surface by capillary pumping provided by a wick structure. Tests have shown that using a heat pipe can boost the system performance by twenty percent when compared to directly illuminating the engine heater tubes.

Designing heat pipe solar receivers has presented several challenges. The relatively large area (~0.2 m^2) of the receiver surface makes it difficult to design a wick that can continuously provide liquid sodium to all regions of the heated surface. Selecting a wick structure with smaller pores will improve capillary pumping capabilities of the wick, but the small pores will restrict the flow of liquid and generate high pressure drops. Selecting a wick that is comprised of very fine filaments can increase the permeability of the wick and thereby reduce flow losses, however, the fine wick structure is more susceptible to corrosion and mechanical damage. This paper provides a comprehensive review of the issues encountered in the design of heat pipe solar receivers and solutions to problems that have arisen. Topics include: flow characterization in the receiver, the design of wick systems, the minimization of corrosion and dissolution of metals in sodium systems, and the prevention of mechanical failure in high porosity wick structures.

INTRODUCTION

The Department of Energy is sponsoring the development of solar-to-electric power-generating systems that use parabolic mirror solar concentrators coupled with a Stirling engine and generator. One of the major challenges of this program is to develop a solar receiver system to transfer energy from the focus of the concentrator to the working fluid of the engine. Flux levels near the focus can be on the order of 100 W/cm^2, and depending on the quality of the concentrator, the flux distribution on the receiver can be very nonuniform. In most solar/Stirling systems, tubes transporting the engine's working fluid are directly heated with concentrated solar energy. This practice creates large thermal gradients on the tubes that can shorten the life expectancy of the receiver system. Uneven flux profiles on the receiver also make it difficult to deliver a balanced thermal input to multi-cylinder engines.

Heat-pipe solar receivers are being developed as an alternative to directly illuminated tube receiver systems. In a heat-pipe receiver system, a wick structure distributes sodium across a solar-heated dome, and thermal energy is removed from the dome as sodium evaporates (see Fig. 1). Sodium vapor condenses on the heater tubes of the engine and energy is transferred to the engine's helium working fluid. Condensed liquid then flows back to the wick-covered evaporator surface under the influence of gravity. Since the sodium is in a saturated state, temperatures within the receiver are uniform and, therefore, thermal stresses are minimized. The concept behind a heat pipe receiver is straightforward, and recent tests by Andraka et al. [1996] demonstrated that a heat-pipe receiver system could improve the

* Sandia is a multiprogram laboratory operated by Sandia Corporation, a Lockheed Martin Company, for the United States Department of Energy under Contract DE-AC04-94AL85000.

DISCLAIMER

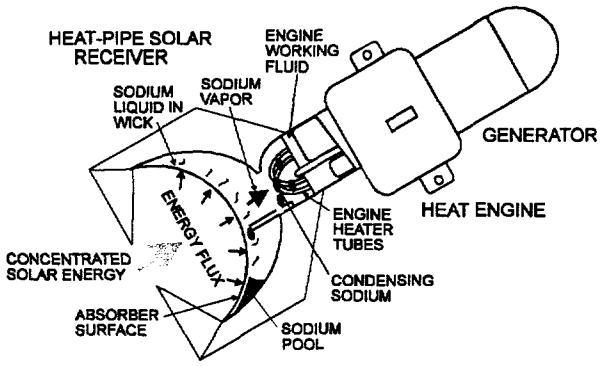

Figure 1. Operating schematic of a heat pipe solar receiver.

efficiency of a dish/Stirling system by 20% over a directly illuminated tube system.

Despite the potential advantages of a heat pipe receiver, system operating requirements have made the receiver development a challenge. Traditionally, there are six recognized limits on the performance of heat pipe systems. First, there is a capillary pumping limit where gravitational and frictional forces exceed the wick's ability to distribute the liquid working fluid by capillary forces. Second is a boiling limit where superheat conditions cause vapor bubbles to form in the wick. Third is an entrainment limit where liquid is suspended by the vapor flow, and prevented from returning to the evaporator wick. Fourth is a vapor velocity limit where friction causes large pressure drops in the vapor ducts between the evaporator and condenser. Finally, there are limits on low temperature operation when the vapor pressure is so low that energy cannot be effectively transported in the vapor phase because of kinetic or sonic restrictions. In addition to operating limits, integrity of the system can be compromised by corrosion of the wick or envelope materials, or the mechanical failure of components at high temperatures. These issues have been investigated in depth over the past 10 years at Sandia and in the labs of several companies involved in the development of commercial Stirling dish-electric systems. The following paper presents conclusions that have been drawn from these years of receiver development activities.

RECEIVER OPERATING LIMITS

Liquid Entrainment and Low Temperature Operation

Energy that is absorbed on the face of the receiver is conducted through the wall and the saturated wick, and then removed by the evaporation of the liquid sodium. At lower temperatures, vapor transport from the surface is kinetically limited; that is, the energy and density of the particles that escape the free surface are insufficient to transport significant quantities of thermal energy. The kinetic limit for mass flux into a vacuum is given by the expression,

$$G = P_{sat} \Big/ \sqrt{2\pi \Re T_{surf}} \qquad (1)$$

where P_{sat} is the saturation pressure at the evaporator surface temperature, T_{surf}, and $\Re$ is the ideal gas constant for the material [Cottrell, 1981]. Multiplying the kinetic mass flux by the latent heat of vaporization yields the kinetic thermal flux limit, $q_{kinetic}$, that is shown for sodium in Table 1. Below about 300°C the evaporative transport is low, so most of the energy goes into raising the temperature of the absorber wall and the wick. The reduced mass and energy transfer rates at lower temperatures allows a receiver system to start from a frozen state without rapidly depleting the sodium supply in the wick. Above about 450°C, the vapor pressure increases sufficiently that the kinetic limit no longer impedes the transport of heat from the surface.

At operating temperatures between 400°C and 600°C, the vapor density is still relatively low, so vapor velocities in ducts connecting the evaporator to the condenser region can be very high. High vapor velocities create large pressure drops within the ducts and this in turn will cause a drop in the vapor temperature. High velocities can also create a situation where the vapor flow is sonically choked. At the sonic limit, the heat flux through a duct with a constant cross-sectional area, A_{duct}, is given by the expression [Shapiro, 1953],

TABLE 1. Properties of sodium [Brennan and Kroliczek, 1979] along with kinetic limits and sonic limits on heat transfer. Specific heat ratio, $\gamma \approx 1.4$, and gas constant, $\Re = 361.6$ J/kgK.

T	P	ρ_v	ρ_l	σ	h_{fg}	ν_v	ν_ℓ	$q_{kinetic}$	q_{sonic}
(°C)	(Pa)	(g/m^3)	(kg/m^3)	(N/m)	(kJ/kg)	(mm^2/s)	(mm^2/s)	(W/cm^2)	(W/cm^2)
200	0.0216	0.0001	903	0.177	4494	1.16×10^8	0.514	0.0094	0.013
300	2.217	0.0011	880	0.168	4421	1.46×10^6	0.393	0.859	0.152
400	55.14	0.231	856	0.159	4344	7.35×10^4	0.326	19.36	33.9
500	561.8	2.08	832	0.150	4259	8740	0.286	180.5	321
600	3310	11.1	809	0.141	4165	1750	0.260	978.5	1780
700	13830	42.6	785	0.131	4067	483	0.238	3781	7040
800	45400	129	761	0.122	3968	168	0.220	11530	21800
900	12160	323	738	0.113	3872	70.6	0.206	28830	55800

$$q_{sonic} = \frac{Q}{A_{duct}} = \rho_v \, h_{fg} \sqrt{\gamma \Re T_v} \left(\frac{2}{\gamma+1} \right)^{\frac{\gamma+1}{2(\gamma-1)}} \qquad (2)$$

where the vapor density, ρ_v, and the latent heat of transformation, h_{fg}, are evaluated at the evaporator temperature, T_v. Sonic flux limits at a few selected temperatures are provided in Table 1. For an evaporator temperature of 500°C, the power that can pass through a 5-cm diameter duct is limited to about 6.3 kW.

In all of the systems that have been tested for the receiver program, pressure drops in the vapor ducts during startup, and the associated temperature drops, have not been found to cause any operating problems. Typical operating temperatures of between 750°C and 800°C for sodium are above the threshold where sonic limits and frictional pressure drops will limit the transport of energy for reasonably sized vapor ducts. We have observed, however, that temperature gradients along the vapor ducts can be on the order of 280°C/cm during the startup process. This transient temperature gradient can put fairly high stresses on the heat pipe walls and it must be considered in material selection and design.

In a typical receiver design, about half of the liquid inventory is held in the wick, and the other half collects in a pool between the evaporator surface and the rear dome of the receiver. At an operating temperature of 700°C and a flux level of 30 W/cm^2, the velocity of vapor leaving the surface is on the order of 2 m/s. Based on a Stokes flow analysis, this velocity is sufficient to suspend sodium droplets with diameters up to 1 mm. Vapor velocities may be further increased by up to two orders of magnitude in duct work to the engine heater heads and narrow passages between the evaporator surface and the rear dome of the receiver (see Figure 1). Flow visualization studies using water in full-scale receiver systems have shown that much of the liquid inventory becomes suspended during the operation of the receiver. Infrared camera images indicate that this phenomenon may also occur in full-scale liquid metal receiver systems. A liquid level is visible in infrared images at temperatures below about 600°C, but the pool line vanishes at temperatures above 600°C. The suspension of the pool has not been observed to adversely affect the operation of the receiver. In most of the receiver systems, however, liquid from the condenser is forced to return directly to the wick structure. Condensate is typically transported through tubes located inside of the vapor ducts between the evaporator region and the condenser region. The condensate tube separates vapor flow from the liquid flow, and thereby prevents the entrainment of liquid. Baffles are also placed in the condenser region cause the vapor to sweep liquid towards the condensate return tubes.

In a few earlier systems, calorimeters were used to extract power and no provisions were made to separate condensate flow from the vapor flow. As a result, liquid would collect in the condenser and vapor ducts, and the wick in the evaporator would periodically be starved for liquid. Entrainment (or "flooding") is especially problematic when the calorimeter extracts excessive power at lower operating temperatures. In calorimeter testing of heat pipes, it is usually not possible to control the extraction of power below some fixed level. Wallis [1969] and Kutateladze [as reported by Tien and Chung, 1978] both offer theories to predict entrainment limits, however, it was found that the Wallis correlation generally over-predicts acceptable power extraction levels. The more conservative Kutateladze expression states that the heat flux at a given cross-section of a circular tube is limited to

$$Q/A = 3.2\xi^{-1/4} \left(D g \rho_l \rho_v \right)^{1/2} h_{fg} \tanh^2 \left(0.5 \xi^{1/8} \right), \qquad (3)$$

where $\xi \left(= D^2 g \rho_l / \sigma \right)$ is the flooding correlation factor. If the heat extraction is above this level, there is a possibility that condensate will not be able to return to the evaporator surface by gravitational forces alone. Since the saturation vapor density increases with temperature, this limit is more restrictive at lower temperatures than at higher temperatures.

Liquid Transport in the Wick and Boiling

Liquid metal is transported over the evaporator surface by the capillary pumping action of the wick, which can be estimated with the expression

$$\Delta P_c = 2\sigma \cos\theta / r_e \, , \qquad (4)$$

where r_e is the effective pore radius of the wick, σ is the surface tension of the liquid, and θ is the wetting angle at the liquid/solid/vapor interface. In general, the wetting angle of sodium on metal surfaces is effectively zero. Capillary pumping must overcome frictional forces and gravity to distribute the sodium. The flow -induced pressure distribution in the wick can be calculated using Darcy's law for flow through a porous medium.

$$\vec{\nabla} P = -\mu_\ell \vec{v} / \kappa_w \, , \qquad (5)$$

where $\vec{v}$ is the superficial velocity of flow through the wick structure, and κ_w is the permeability of the wick [Bird, Stewart, and Lightfoot, 1960].

Complex flux distributions make it necessary to solve for the pressure distribution using a finite element approach. A general understanding of the solution approach can be obtained by considering the element mesh illustrated in Figure 2. Based on continuity considerations, the net flow that passes through the wick element is equal to the evaporation from the surface of the element. This can be written as,

$$\dot{m}_{21} + \dot{m}_{31} + \dot{m}_{41} + \dot{m}_{51} = q_1 \Delta x \Delta y / h_{fg} = q_1 S_1 / h_{fg} \, . \qquad (6)$$

From Darcy's law (Eq. 5), the pressure difference between point 0 and point 1 is,

$$\Delta P_{21} = -\frac{\mu_\ell}{\kappa} \Delta y \frac{\dot{m}_{21}}{\rho_\ell \delta \Delta x} = -\nu_\ell \dot{m}_{21} / K_{21} \, . \qquad (7)$$

Similar expressions can be written for the flow between Point 1 and Points 3, 4 and 5. Equations 6 and 7 are combined to yield,

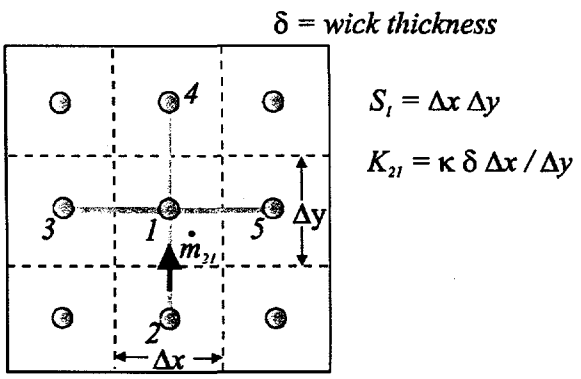

Figure 2. Mesh for the development of finite element equations for pressure calculations.

$$K_{21}\Delta P_{21} + K_{31}\Delta P_{31} + K_{41}\Delta P_{41} + K_{51}\Delta P_{51} = -q_1 \nu_\ell S_1 / h_{fg} \qquad (8)$$

After expressions are written for all N elements, there will be N equations for N unknown pressures. The resulting pressure distribution considers frictional pressure drops alone; gravitational head must be deducted (or added) to get the final pressure distribution in the wick. For the spherical-dome shaped wicks that are now used on most heat pipe receivers, the flow coefficients K_{ij} and the elemental surfaces, S_i, must be modified to reflect the spherical geometry (see Adkins [1988] for details).

For the simple case where a dome-shaped receiver is in a vertical orientation (with the open cavity facing down) and is fed from a pool along the perimeter edge, the pressure distribution in the wick is given by the expression,

$$P_\alpha - P_p = -\left(\frac{2\nu_\ell q}{\kappa_w \delta h_{fg}}\right) R^2 \ln\left(\frac{\cos[\alpha/2]}{\cos[\alpha_p/2]}\right) - \rho_\ell g R\left(\cos\alpha - \cos\alpha_p\right) \qquad (9)$$

where P_p is the pressure at the perimeter pool, q is the uniform flux on the surface, R is the receiver radius and α is the angle measured from the center-line of the dome (see Figure 3). Two observations can be made about this expression: *First, the pressure drop is inversely proportional to the product of the permeability and the wick thickness.* If the permeability of the wick is doubled, then the thickness can be halved, and this in turn will reduce the temperature drop across the wick *Second, the pressure in the wick is always lower than the vapor pressure.* Liquid within the wick will be in a superheated state, and the superheat is further increased when heat must be conducted through the wick. Fortunately, liquid metals can withstand high superheat conditions without boiling, but it is always possible that some vaporization will occur in the wick.

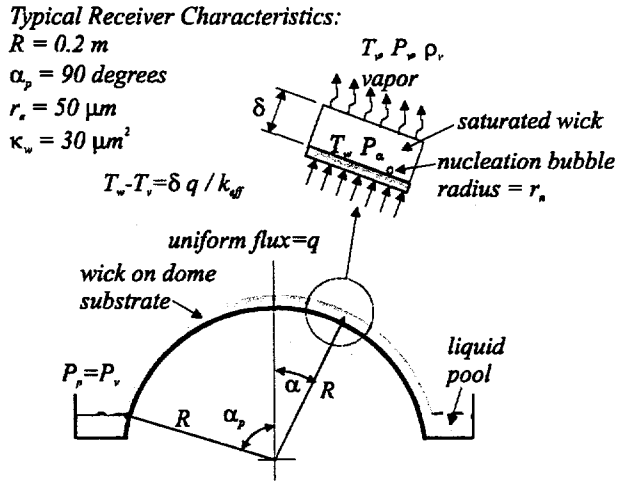

Figure 3. Dome receiver in a vertical orientation subjected to a uniform thermal flux.

The capillary pumping capability of the wick is traditionally based on some average effective pore radius for the wick. Capillary pumping is compared with the frictional and gravitational pressure drop to determine the operating power limit for the heat pipe. A second power limit is established by comparing the superheat conditions in the wick to the temperature drop across the wick. The critical superheat limit is usually based on the stability of a nucleation site within the wick. The critical temperature difference between the liquid temperature in the wick and the local vapor temperature is given by the expression [Chi. 1976],

$$\Delta T_{crit} = \left[\frac{2\sigma}{r_n} - \left(P_v - P_\ell\right)\right] \frac{T_v}{h_{fg}\,\rho_v} \quad . \qquad (10)$$

where P_ℓ is the liquid pressure in the wick and P_v is the saturation vapor pressure. The radius of this nucleation site, r_n, is usually not known, so the usefulness of this expression in design applications is limited. Chi [1976] suggests that the radius of a nucleation site may range from 0.25 to 25 μm for clean heat pipe systems.

For the receiver properties listed in Figure 3, the capillary pumping pressure at 800°C would be approximately 4.9 kPa based on Eq. 4, and the predicted flux limit based on Eq. 9 would be 33 W/cm^2. If the effective conductivity in the wick were 42 W/mK, then nucleation sites of 10 μm or smaller would be stable at this flux level based on the critical temperature expression in Eq. 10. These calculations, of course, are for the orientation that is illustrated in Figure 3. If the receiver axis is horizontal and the pool is at the bottom of the receiver, then liquid will be required to flow further through the wick, and superheat conditions will increase.

The traditional design approach outlined above provides useful insights into building receivers, but the results can be overly conservative for many wick structures. Most wicks have a distributed pore structure as opposed to the single effective pore

radius considered in the traditional model. The distributed pore structure means that the wick will not fail at a specific flux, but it will gradually degrade as flux levels increase. When the pressure in the wick decreases as a result of thermal flux or gravity loading, the larger pores will fill with vapor, but the smaller pores will continue to transport liquid. Frictional pressure drops in the wick will increase, but the temperature drop across the wick will decrease because of the reduction in the heat conduction path length and the effective increase in the evaporative surface area presented by the exposed wick material [Rosenfeld, 1989]. A more complete description of liquid transport in wicks in the presence of vapor formation is provided by Shaubach, Dussinger and Bogart [1990] and application of these concepts to dome-shaped receiver surfaces is offered by Andraka [1999].

Wick Properties

From a thermal transport standpoint, the ideal wick would have a micron-sized pore structure for high capillary pumping capabilities, and it would be nearly 100 percent porous to minimize flow losses through the wick. Pores in the wick would also be graded so vapor bubbles that may form near the heated surface could migrate to the wick surface and escape rather than remain in the wick and block the flow of liquid. This ideal wick could be envisioned as a cubic lattice made of infinitely fine wires that are separated by a few microns near the heated surface and open up to a few tens of microns towards the wick's free surface. For the half-meter diameter hemispheres that are being developed for 75-kW solar receivers, the wick permeability should be on the order of 30 to 100 μm^2.

To model the receiver, it is necessary to know the permeability and the pore radius of wick material. Empirical relationships for these properties in low porosity materials, such as powdered metals and screens, are provided by Dunn and Reay [1982], Chi [1976], and Brennan and Kroliczek [1979]. For more porous materials, such as felt metals, Jackson and James [1986] have compiled a literature review on experimental measurements and theoretical models of permeabilities, and Ranganathan, Phelan, and Advani [1996] discuss numerical simulations of flow though fiber structures.

Wick models may show how parameters, such as particle size, wire diameter, or porosity, will affect the permeability and effective pore size of the wick material, but more precise information is usually required to design receiver systems. Permeability measurements can be made with the simple system that is illustrated in Figure 4 where a liquid (such as methanol) is forced to flow through the wick structure in a radial direction. The permeability is calculated using the expression,

$$\kappa = C_{2D} \frac{v\dot{V} \ln(r_o/r_i)}{2\pi g H \delta} \qquad (11)$$

where v is the liquid velocity, and $\dot{V}$ is the volumetric flow through the system, and C_{2D} is a correction factor for the two-dimensional effects at the inlet. When r_o is much larger than r_i the correction factor is near 1. For r_o =30 mm and r_i =10 mm, the

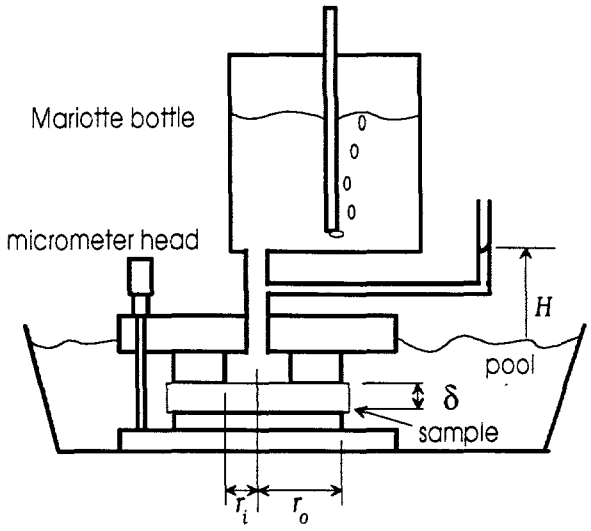

Figure 4. Permeability measuring rig.

correction was found through numerical simulations to be $C_{2D} = 1 + 0.027\,\delta + 0.005\,\delta^2$ where the thickness, δ, is in millimeters [Adkins et al., 1995].

Pore distributions in wick structures are typically measured using porometry [ISO 4793-1980] or mercury porosimetry [A.S.T.M. 4404-84]. With mercury intrusion porosimetry, mercury is forced into an evacuated sample, and the pressure is measured as a function of the volume of mercury that enters the sample. In porometry, gas is forced to flow through a liquid-saturated sample and the pressure drop across the sample is measured as a function of the flowrate. The point where gas first passes through the wick is referred to as the bubble point pressure, and the corresponding bubble point pore radius represents the largest continuous path through the material. Inherent errors exist in both mercury porosimetry and porometry measurements. Large interior cells that are enclosed by small surrounding cells will skew porosimetry and porometry results toward a higher count of smaller pores. In the receiver design program, it is recognized that measured pore distribution is an approximation. The practice that was eventually adopted for receiver design was to approximate the pore radius as a linear distribution between 5 μm and the bubble point radius based on porometer data. When this approximate distribution was used with Andraka's [1999] vapor loaded wick model, it was found that model predictions were accurate to within 5 percent of the measured operating power limit.

MECHANICAL PERFORMANCE

The receiver shell must provide a hermetic envelope at all operating temperatures for the system to function properly. If non-condensable gases are present, the gas will interfere with the flow of vapor and create a large temperature drop in the condenser region at normal evaporator operating temperatures. A large temperature difference between the evaporator and condenser is frequently the first indication that a leak has occurred in the system. It can also indicate that a gas, such as hydrogen, has diffused through the wall of the receiver. Hydrogen diffusion was a

persistent problem in earlier gas-fired heat-pipe systems, but this problem can be avoided by operating with lean fuel/air mixtures (50% excess air) [Adkins and Rawlinson, 1992]. If air enters the heat pipe, then the introduced oxygen will rapidly combine with sodium and the resulting compound is extremely corrosive at elevated temperature. (Corrosion mechanisms are discussed later.)

Type 316L stainless steel was used to form the shell or "envelope" in several of the early prototype receivers. It was generally observed that mechanical stress levels exceed recommended design limits for this material. Later designs used a nickel-based super alloy (Haynes 230) which, compared to stainless steels, has superior mechanical strength and airside corrosion resistance at elevated temperatures. Type 316L stainless steel fibers, or nickel powders were used as wick materials in most of the devices that were tested. Currently, it appears that metal felts made of 8-μm diameter wires applied at a surface density of 900 g/m^2 and compacted to 4-mm thick provides the best wick structure. Felt is attached to the receiver dome by sintering at 1150°C in vacuum for 1 hour. Grit blasting the receiver surface has been found to improve the sinter bond. Gas tungsten arc welding is used in constructing the heat-pipe envelope whenever possible, but joints with boron-nickel based brazes have also been used in the sodium environment. Breaches at both welds and high flux areas of the evaporator were observed in a few of the initial test heat pipes. Since switching to Haynes 230, however, no structural failures have been observed in the envelope. Corrosion in the wick structure, and mechanical failure of the wicks are the two most frequently encountered problems with heat pipe receivers.

Wick Corrosion and Corrosion Mitigation

Corrosion and material compatibility issues in liquid-metal systems have been studied extensively in relation to nuclear power reactors, and reviews of this work are provided by Foust [1972], Barker and Wood [1974], and Natesan [1975]. A general finding from this work is that stainless steels and refractory metals have solubilities below a few ppm in pure liquid metals, even at elevated temperatures. Impurities such as oxygen, however, can drastically increase the dissolution rates of stainless steels [Barker and Wood, 1974]. It is hypothesized that the accelerated dissolution rates are a result of the formation of ternary compounds, such as $NaCrO_2$ or Na_4FeO_3, that are relatively soluble in liquid metals [Lundberg, 1987].

While research for liquid-metal reactors is applicable to heat pipe systems, there are unique differences. Typical sodium reactor systems were designed for operating temperatures below 600°C, whereas sodium heat pipe systems usually operate at temperatures above 700°C. The evaporative action of the heat pipe also works to concentrate contaminants on the evaporator wick surface. Los Alamos National Laboratory has been somewhat successful in modeling the corrosion process in heat pipes, but limited thermochemical data hinders the predictive capability of the model [Merrigan and Feber, 1985].

The combined effects of an increased material solubility with oxygen levels and the action of the heat pipe to concentrate impurities, such as oxygen, creates a situation where the wick structure in the evaporator is extremely vulnerable to damage. Natesan's review of corrosion in liquid metal systems found that corrosion rates in liquid metals vary linearly with oxygen concentration. A 1-ppm oxygen concentration in sodium could cause corrosion rates on the order of 1 micron per year on stainless steel, and a 10-ppm concentration could cause a 10 micron per year rate under the same temperature and flow conditions. Most of the oxygen contamination is introduced into the system on the surface of the wick [Ivanovsky et al., 1995]. For a typical heat-pipe receiver system, oxides on the felt wick surface can raise the overall oxygen levels in the sodium to about 100 ppm by weight if steps are not taken to reduce the native oxide layer.

In the receiver development program, significant corrosion damage has been observed even in systems that have operated for only tens of hours. Typically, a portion of the wick will be completely destroyed in a small area (~5-mm diameter) and a larger surrounding area will be covered with deposits. The deposits are usually sodium and aluminum oxides, but elemental deposits of molybdenum and tungsten will also form on the wick. When felt-metal wicks are used in receivers, there has also been a persistent problem of copper nuggets forming on the evaporator wick (Copper sleeves are apparently used in drawing the stainless steel fibers, and a trace amount of the copper remains after cleaning in nitric acid.) Nodules of chrome often appear on the wick surface in the pool region. Facets appear on felt-wick structures throughout the heat pipe, and it is especially pronounced on the evaporator wick. Many of these features are shown in the photographs in Figure 5 and 6.

The exact mechanism for corrosion failure is not fully understood, but, based on the cited literature and the results from many systems tested in the receiver development program, the following failure scenario can be put forward. The corrosion process begins as sodium vapor condenses on the cooled condenser surface. The condensed sodium is fairly pure, so oxygen from the chromium oxide layer on the wick surface would readily go into solution. As the oxygen contaminated sodium flows from the condenser to the pool, elemental constituents of the wick material begin to go into solution. Chromium is known to have a fairly high solubility in oxygen-contaminated sodium, and iron is also soluble, but slightly less so [Foust, 1972]. (The solubility of nickel in oxygen-contaminated sodium is uncertain, and results provided by Foust are contradictory.) Condensed sodium flows to the pool, and, if the liquid cools, some of the metals precipitate from solution. An oxygen getter material such as zirconium may remove some of the oxygen in the sodium pool, but the process is diffusion limited and the getter can become saturated. Liquid sodium from the pool, which is still contaminated with oxygen, is transported by capillary pumping through the wick structure to the evaporator surface. As the liquid flows to the evaporator surface, oxygen and other material from the wick structure goes into solution and gets transported to the evaporator area. Liquid sodium evaporates away in the heated area and leaves behind the dissolved metals and oxide compounds with low vapor pressures. The metallic residues begin to collect in the evaporator wick structure and block the flow of liquid sodium. Oxide compounds are gradually swept to the top of the evaporator section where they concentrate. Eventually, the concentrated oxide compounds corrode away a section of the wick, and, without a supply of liquid sodium; the surface that was previously covered by the destroyed wick overheats.

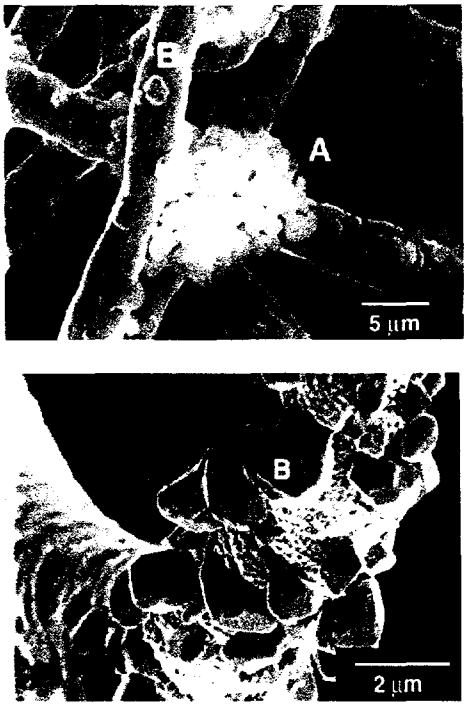

Figure 5. Felt metal wick from a sodium heat pipe after 1995 hours of operation. The heat pipe was vacuum baked at 700°C for 4 days prior to filling with a charge of sodium. (Top) evaporator wick with calcium-oxide (A) and sodium-oxide deposits (B). (Bottom) pool wick with chrome nodules (B).

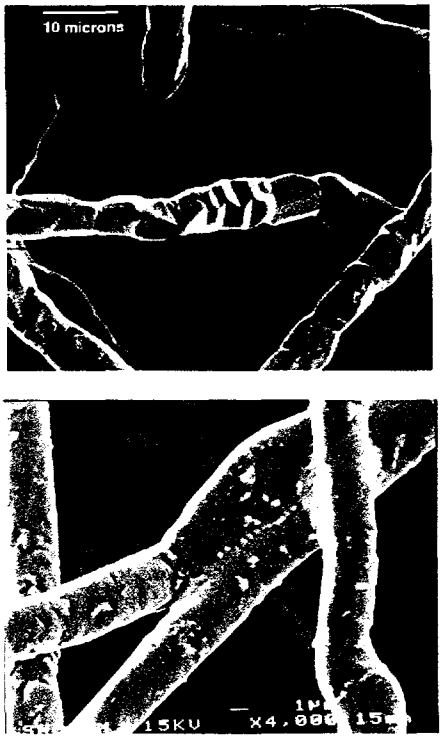

Figure 6. Felt metal wick from a sodium heat pipe after 1300 hours of operation. The heat pipe was reflux cleaned for 6 hours prior to filling with a charge of sodium. (Top) evaporator wick shows facetted surface, but no deposits. (Bottom) pool wick shows scattered flecks of molybdenum, but no chrome nodules that were observed on the system that was cleaned by vacuum baking alone (see Fig. 5).

By comparing diffusion rates to the liquid transport rates through the wick, it can be shown that the evaporative action of the receiver will concentrate contaminants by a thousand-fold above initial contamination levels [Adkins, et al., 1998]. It can further be shown that the peak concentration of contaminants is proportional to the thermal flux, and the contaminants will concentrate to a centimeter-sized region where maximum wick damage will occur. This estimated concentration area correlates well with observed damage on full-scale receivers.

Heat pipes are typically cleaned through flushing techniques or high-temperature vacuum bakeouts. Vacuum bakeouts will not be effective unless temperatures are high enough to reduce the native oxides. For processing sodium heat pipes, Woloshun [1997] reports using vacuum firing temperatures of 1127°C. and it is suggested that this temperature is effective in removing oxygen from the system. Mausteller, et al. [1967] indicates that carbon in stainless steels reduces oxides and forms CO at elevated temperatures. CO is observed to be the dominant residual gas released from heat pipes that are vacuum fired at temperatures above 950°C. Even at firing temperatures of 1127°C, however, Woloshun [1997] indicates that vacuum baking can take on the order of a week.

Oxides can be reduced at lower temperature by providing a reactive atmosphere in the heat pipe. Hydrogen firing is traditionally used to reduce surface oxides, but this practice will introduce hydrogen into the systems that can be difficult to remove [O'Hanlon, 1980]. Another option is to use the reactive liquid metal itself to flush the system clean and transport contaminants to separate loops where they can be trapped. Mausteller, et al. [1967] provide a practical guide to cleaning liquid metal systems through flushing and trapping contaminants, and Stelman and Newcomb [1993] describe the use of such a system for cleaning heat pipes. In processing their system, Stelman and Newcomb vacuum baked the heat pipe at 427°C, soaked the interior of the vessel for 24 hours in sodium at 427°C, and then flushed the heat pipe for 48 hours with hot sodium. The hot soak and flushing is repeated at least three times to achieve oxygen concentrations below 10 ppm in the drained sodium.

Like vacuum baking, the flushing procedures described by Stelman and Newcomb took a week or more to complete. The process could be accelerated by increasing the flushing temperature and by ensuring that the process does not become diffusion limited. Areas of stagnant liquid will prevent the effective transport of oxygen from the surface and lengthen processing times. Rather than flushing liquid through the vessel, directly condensing the liquid on the surface will ensure that the liquid near the contaminated surface is pure, and diffusion distances are minimized.

Several techniques have been tested at Sandia National Laboratories for their effectiveness in cleaning sodium heat-pipe systems. Early systems were vacuum baked at 700C for four days before filling with a charge of sodium. This process was ineffective in cleaning the system as Figure 5 illustrates. The most effective procedure has been to bake the system for 72 hours at 600°C under an internal vacuum, and then to flush the system for six hours by condensing 600°C sodium vapor on the interior surfaces [Adkins et al, 1998]. This procedure reduces corrosion damage to the wick and slows the formation of deposits (see Figure 6). The long-term (>10,000 hours) effectiveness of this process is currently being examined in several heat-pipe life-cycle tests at Sandia National Laboratories.

Mechanical Degradation and Failure Mitigation

As was previously stated, the wick should have very fine structure that will minimize interference with the flow of liquid for optimum thermal performance. Unfortunately, this same characteristic will make the wick vulnerable to corrosion and mechanical failure. Two types of mechanical damage to the wick have been encountered in the receiver development program: (1) eruptive failures where portions of the wick are lifted from the surface, and (2) crushing failures where the wick collapses toward the surface.

Eruptive failures have occurred with both powdered metal wicks and felt metal wicks. Generally, these failures appear as a cavern beneath the wick surface, and often these caverns create raised areas on the surface, about 3-cm in diameter, with radial cracks appearing in the wick surface. Typically, the damage is within the wick structure, and not at the substrate/wick interface. The initiation mechanism for the eruptive failures is still unknown, but it is possible to estimate of the pressure required to split the wick open once a cavity is present. If it is assumed that the cavity is a spherically shaped void of radius R_{cavity}, then the minimum pressure required to rupture the wick would be,

$$\Delta P_{rupture} = \frac{2\,\delta\,\sigma_{ult}}{R_{cavity}}$$

where δ is the zero porosity thickness of the wick material forming the cavity wall. The ultimate stress for wick materials, σ_{ult}, generally is not available, however, pull-tests were performed on felt metal samples, and the results are shown in Figure 7. The strength of this material is a function of the sintering temperature, and the compaction of the material during the sintering process. Sintering at higher temperatures in a more compacted state increases the bond formation between contacting fibers. For most of the felt wicks that have been tested in receivers, the ultimate stress is on the order of 40 MPa at room temperature. For 316 steel, the ultimate strength at 800°C is about one-third the strength at room temperature to 25 ksi at. If it is assumed that the strength for felt metals scales in a similar manner, then σ_{ult} equals 13 MPa at 800°C. This implies that a 4/150 felt wick with a 2-cm diameter cavity would fail at 48 kPa pressure difference.

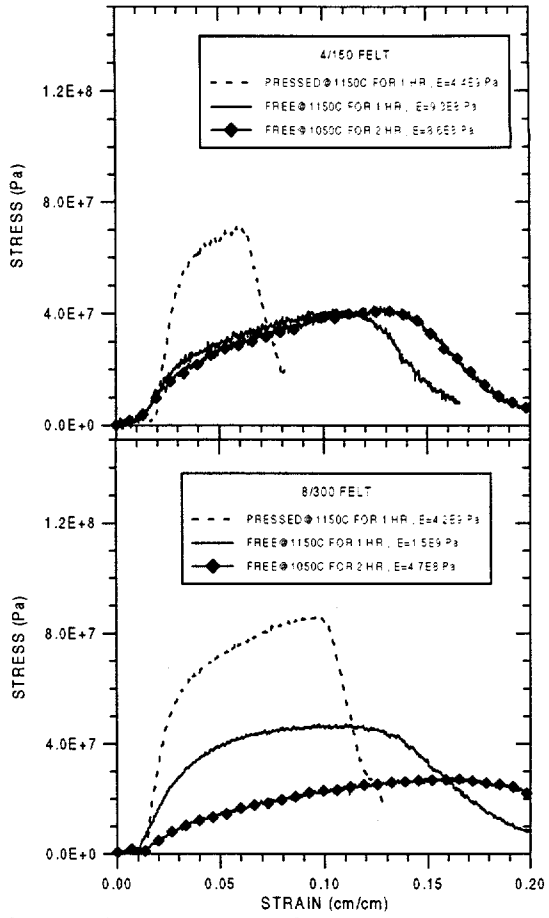

Figure 7. Pull test results on Bekaert Fibres 4/150 and 8/300 felt metal materials. Samples were sintered in both a unrestrained (free) condition and a fully compressed condition. The fully densified thickness that was used to determine stress was 38.2 μm for the 8/300 felt, and 19.1 μm for the 4/150 felt.

At 810°C, the vapor pressure of sodium is 50kPa, so it is conceivable that a 48 kPa pressure difference could occur during transient situation when the evaporator temperature is high (>800°C) and the vapor temperature in the receiver is low (<600°C). The inflation of the vapor bubble would have to be rapid, though, to avoid simply venting the gas through the porous structure. Surface tension could play a role in trapping the vapor in the wick, but to hold back a pressure of 46 kPa, the effective pore radius would have to be on the order of 5 μm or less. In addition to vapor generation, a sudden pressure pulse could also be caused by the rapid decomposition of sodium hydrides [Foust, 1972]. Our efforts to experimentally recreate a sodium hydride explosion in a sodium saturated wick, however, were not successful.

Wick crushing has only been observed in heat pipes with felt metal wicks, but it is likely that any high-porosity, fine-element wick structure will experience the same problem. All evidence indicates that the crushing is caused by surface tension pulling the wick toward the substrate. Wick crushing damage is the greatest in areas of high fluxes, and low liquid pressures. Sub-scale heat pipe

tests have shown that mounting a perforated metal shell over the wick structure can eliminate crushing damage. The perforated shell is typically bonded to the wick through sintering. Prior to sintering, the surface of the perforated metal is sandblasted to improve adhesion. Tests are now underway to determine if this approach will be suitable for full-scale receiver systems.

Recent tests have indicated that eruptions on the wick surface may be linked to the crushing in the wick caused by surface tension. On a bench-scale system with a felt-metal wick, X-ray images showed that during the first 10 hours of operation the wick collapsed in towards the substrate. After 100 hours of operation, however, the collapsed area expanded to about double the original thickness. Near the evaporative surface, the wick was about 82% porous, but in the expanded area, the wick was about 97% porous. The lower porosity near the surface of the wick would make it more difficult for vapor or trapped gases to escape. If the original crushing of the wick could be mitigated with a porous metal shell, then the subsequent eruption problems may also be reduced.

CONCLUSIONS

Heat-pipe solar receivers offer an efficient alternative to transfer heat from the focus of a parabolic dish collector to the heater-tubes of a Stirling engine. Through 10 years of design innovations, many of the problems associated with the receiver have been overcome. Models are now available that provide an accurate estimate of the performance of solar receivers. Procedures have also been developed for measuring wick properties that are required for the receiver model. Currently, felt metal materials appear to offer the best mix of high permeability and low pore radius properties for the receiver wicks. The fine structural elements of the felt metal materials provide excellent transport characteristics, but the same fine features make felt metals susceptible to corrosion and mechanical damage. It appears that surface tension forces crush the wick during operation, but there is evidence that sintering a perforated metal support structure over the wick surface can eliminate crushing. The support structure may also eliminate incidents where the wick is torn apart at the surface, but, at this time, there is not a full understanding of the cause of the surface eruptions. Corrosion continues to pose some concern in the receiver development program. However, it appears that cleaning the interior surface with condensing high temperature sodium can significantly reduce corrosion damage.

ACKNOWLEDGEMENTS

The authors would like to thank Daniel Ray and Walter Einhorn for their years of assistance in building and testing heat pipes. Sandia is a multiprogram laboratory operated by Sandia Corporation, a Lockheed Martin Company, for the United States Department of Energy under contract number DE-AC04-94AL85000

REFERENCES

Adkins, D. R., Rawlinson, K. S., Andraka, C. E., Showalter, S. K., Moreno, J. B., Moss, T. A., and Cordiero, P. G., 1998, "An Investigation of Corrosion in Liquid-Metal Heat Pipes," *Proceedings of the Mechanical Engineering Congress and Exposition*, Heat Pipes and Thermosyphons Session, Anaheim, CA, November, 15-20.

Adkins D. R., Andraka, C. E., Bradshaw, R. W., Goods, S. H., Moreno, J. B., and Moss, T. A., 1996, "Mass Transport, Corrosion, Plugging, and Their Reduction in Solar Dish/Stirling Heat Pipe Receivers," *Proceedings of the 31st IECEC*, Vol. 2, pp. 1307-1311, Washington, D.C.

Adkins, D., Moss, T., Andraka, C., Cole, H., and Andreas, N., 1995, "An Examination of Metal Felt Wicks for Heat-Pipe Applications," ASME/JSME Solar Engineering Conf., Maui, HA.

Adkins, D. R., and Rawlinson, K. S., 1992, "Design, Fabrication, and Testing of a 15-kW Gas-Fired Liquid Metal Evaporator," *Proceedings of the 27th IECEC*, San Diego, CA, Aug. 3-7.

Adkins, D. R., 1988, "Analysis of Heat Pipe Receivers for Point Focus Concentrators," Sandia National Laboratories, Albuquerque, NM, SAND88-0093.

Andraka, C., Rawlinson, K., Moss, T., Adkins D., Moreno, J., Gallup, D., and Cordeiro, P., 1996, "Solar Heat Pipe Testing of the Stirling Thermal Motors 4-120 Stirling Engine," *Proceedings of the 31st IECEC*, Vol. 2, pp. 1295-1300, Washington, D.C.

Andraka, C. E., 1999, "Solar Receiver Wick Modeling," Submitted for the *Proceedings of the 1999 Solar Energy* Conference, Maui, HA.

Barker, M. G., and Wood, D. J., 1974, "The Corrosion of Chromium, Iron, and Stainless Steel in Liquid Sodium," *J. of Less-Common Metals*, Vol. 35, pp. 315-323.

A.S.T.M. 4404-84, "Standard Test Method for the Determination of Pore Volume and Pore Volume Distribution of Soil and Rock by Mercury Intrusion Porosimetry," published 1984, reapproved 1992.

Bird, R. B., Stewart, W. E., and Lightfoot, E. N., 1960, *Transport Phenomena*, John Wiley and Sons, Inc. NY.

Brennan, P. J., and Kroliczek, E. J., 1979, "Heat Pipe Design Handbook: Volume I," NTIS Pub. No. N81-70112.

Brennan, P. J., and Kroliczek, E. J., 1979, "Heat Pipe Design Handbook: Volume II," NTIS Pub. No. N81-70113.

Chi, S. W., 1976, *Heat Pipe Theory and Practice: A Sourcebook*, Hemisphere Publishing Corp., Washington.

Cottrell, A. H., 1981, *The Mechanical Properties of Matter*, Robert E. Krieger Publishing Co., Huntington, NY, pp. 58.

Dunn, P. D., and Reay, 1983, *Heat Pipes*, 3rd ed. Pergamon Press, Oxford, UK.

Dunn, P. D., and Reay D. A., 1982, *Heat Pipes, 3rd ed.*, Pergomon Press, NY.

Foust, O. J., ed., 1972, *Sodium-NaK Engineering Handbook, Volume 1, Sodium Chemistry and Physical Properties*, Gordon and Breach, Science Publishers, Inc., 440 Park Ave. So., New York, NY.

Ivanovsky, M. N., Morozov, V. A., and Shimkevich, A. L., 1995, "On Advanced Technology of Fluids for Heat Pipes," *Proceedings of the IX International Heat Pipe Conference*, Albuquerque, NM.

Jackson G. W., and James, D. F., 1986, "The Permeability of Fibrous Porous Media," *The Canadian Journal of Chemical Engineering*, Vol. 64, June, pp. 364-374.

Lundberg, L. B., 1987, "Alkali Metal Heat Pipe Corrosion Phenomena," *6th International Heat Pipe Conference*, Grenoble, France.

Mausteller, J. W., Tepper, F., and Rodgers S. J., 1967, *Alkali Metal Handling and Systems Operating Techniques*, Gordon and Breach, Science Publishers, NY.

Merrigan, M. A., and Feber, R. C., 1985, "Thermochemical Correlation of Transport in an Alkali Metal Heat Pipe," Los Alamos Report No. LA-UR-85-2648.

Natesan, K., 1975, "Interactions Between Structural Materials and Liquid Metals at Elevated Temperatures," *Metallurgical Transactions A*, Vol. 6A, pp. 1143-1153.

O'Hanlon, J. F., 1980, *A Users Guide to Vacuum Technology*, John Wiley & Sons, Inc., NY.

ISO4793-1980, "Laboratory Sintered (Fritted) Filters – Porosity Grading" issued 1980.

Ranganathan, S., Phelan, F., R., and Advani, S. G., 1996, "A Generalized Model for the Transverse Fluid Permeability in Unidirectional Fibrous Media," Polymer Composites, Vol. 17, No. 2, April, pp. 222-230.

Rosenfeld, J. H., 1989, Nucleate Boiling Heat Transfer in Porous Wick Structures, HTD-Vol. 108, pp 47-55.

Shapiro, A. H., 1953, *The Dynamics and Thermodynamics of Compressible Fluid Flow, Vol. 1*, John Wiley & Sons, NY, pp. 85.

Shaubach, R. M., Dussinger, P. M., and Bogart, J. E., 1990, "Boiling in Evaporator Wick Structures," *Proceedings of the 7th International Heat Pipe Conference*, Minsk, USSR.

Stelman, D., and J. C. Newcomb, 1993, "Filling and Sealing Sodium Heat Pipes," CONF 930103, Am. Inst. of Physics, pp. 533-538.

Tien, C. L., and Chung, K. S., 1978, "Entrainment Limits in Heat Pipes," AiAA Paper 78-382, *Proceedings of the 3rd International Heat Pipe Conference*, Palo Alto, CA.

Wallis, B. B., 1969, *One Dimensional Two Phase Flow*, McGraw-Hill Book Co.

Woloshun, K., 1997, "KAPL Heat Pipe Technology Program," presentation at the KAPL High Temperature Heat Pipe Meeting, Knolls Atomic Power Laboratory, Schenectady, NY, Nov. 16-18.